Algorithm for Analyzing the Microenvironment Surrounding Melanoma

Tăbăcaru Gigi
Department of Automatic Control and Electrical Engineering
Faculty of Automation, Computers, Electrical Engineering and Electronics,
"Dunarea de Jos" University of Galati,
47 Domneasca Str. 800008
Galati, Romania
gigi.tabacaru@ugal.ro

Moldovanu Simona
Computer Science and Information Technology, The Modelling & Simulation Laboratory,
Faculty of Automation, Computers, Electrical Engineering and Electronics,
"Dunarea de Jos" University of Galati,
47 Domneasca Str., 800008
Galati, Romania
simona.moldovanu@ugal.ro

Barbu Marian
Department of Automatic Control and Electrical Engineering
Faculty of Automation, Computers, Electrical Engineering and Electronics,
"Dunarea de Jos" University of Galati,
47 Domneasca Str. 800008
Galati, Romania
marian.barbu@ugal.ro

Abstract — **Peritumoral areas or microenvironments surrounding melanoma are unexplored and partially understood, so the following paper proposes an algorithm that predicts the trend of melanoma progression. Additionally, in the case of melanoma, the peritumoral area is significantly correlated with the texture that belongs inside the skin lesion. The proposed algorithm analyzes the region of interest (ROI) with the Normalized 2-D cross-correlation (NCC) method and predicts the pattern in the peritumoral area, which is most similar to the texture of the melanoma. An important step is detecting the peritumoral area, in which case the mathematical morphology techniques were proposed. The Structural Similarity Index (SSIM) was used to compare the similarity of samples taken from inside the melanoma and the peritumoral area. The main advantage of the proposed algorithm is that it can be applied to different medical image types and tumors. The algorithm was tested on two datasets, 7-Point and PH2, and two computers.**

Keywords: peritumoral area, Normalized 2-D cross-correlation, Structural Similarity Index

I. INTRODUCTION

Melanoma is a skin lesion that includes a variety of color clusters and texture patterns. The World Health Organization stipulated in 2020 that melanoma and other skin cancers affect mostly people over 75 years of age. In the world, the number of new cases of skin lesions annually is 324,624 and the number of deaths is 57,043 for both sexes and all ages. The most affected population in the world is the one living in Northern America. The main cause of skin cancer is caused by ultraviolet radiation [1].

The proposed study became important because it brings forth contributions to monitoring the spread of melanoma and expresses a relationship between the intratumoral and peritumoral areas. The early detection of this dangerous skin lesion allows the patient to recover and live a quality life. The accessibility of the patient to the latest technology results in the acquisition of images of the best quality; therefore, using the processing tools, the best algorithms for detecting the different areas of melanoma or those surrounding it can be implemented .

The Graph Cut Segmentation Method (GCS) partitions the dermoscopic image into meaningful compartments, and it was also used successfully in many studies [2], [3] and [4] for the segmentation of ROIs. Other important processed image methods are mathematical morphology, the erosion and dilation methods employed in combination with structuring elements into fixed patterns, which are very useful in medical images [5].

A 2D NCC method generates cross-correlation maps between a template and a region of interest [6]. NCC based on the Sobel operator by Liu *et al.* [7] was proposed, with their method evaluating tissue damage and improving the targeting of lesions by increasing the visual surgery field. The CNN technique is presented in the paper [8], the authors used the extraction of spatial and spectral features from ROI and the Gaussian Laplacian operator to introduce a new similarity measure for increasing of internal detail. This combination leads to the best solution provided by CNN.

The SSIM index is applied when the similarity between two images is verified. In image processing, it is a useful metric for the measurement or prediction of image quality based on its texture [9]. In the field of dermoscopy, the artifacts affect the quality of images, and these are improved with different filters. The improvement of images after the hair is removed was measured with the SSIM index [9].

The microenvironment surrounding the skin lesion plays an important role in melanoma progression because this area gives signals regarding tumor growth, motility, and metastasis [10] and [11]. Because the domain is very important in this work, major contributions were made as follows: (i) pattern detection in the peritumoral area of melanoma with NCC; (ii) Detection of the similarity between template cropped forms inside ROI on the peritumoral area with SSIM; (iii) Prediction of the progression of melanoma with the magnitude spectrum of dermoscopic images; (iii) Testing the proposed algorithm on two computers with different architectures; and (v) Estimating the number of samples from each image and keeping track of them.

II. MATHEMATICAL APPROACHES

After having projected the implemented algorithm, two metrics, NCC and SSIM, were proposed.

1. Normalized cross-correlation is a useful metric for the quantification of the template similarity with a ROI.

$$NCC(I,J) = \frac{\sum_m \sum_n [I(m,n) - \overline{I_{m,n}}][J(x-u,y-v) - \overline{J}]}{\left\{\sum_m \sum_n [I(m,n) - \overline{I_{m,n}}]^2 \sum_m \sum_n [J(x-u,y-v) - \overline{J}]^2\right\}^{0.5}} \quad (1)$$

I is the image, J is template, $\overline{J}$ is the mean of the template J, $\overline{I}$ is the mean of I in the region under the template J [12].

2. The Structural Similarity Index (SSIM) measures the perceived changes in structural information, and it is computed using the luminance (l), contrast (c), and structural texture (s) [13].

$$SSIM(x,y) = [l(x,y)]^\alpha \cdot [c(x,y)]^\beta \cdot [s(x,y)]^\gamma \quad (2)$$

where

$l(x,y) = \frac{2\mu_x \mu_y + C_1}{\mu_x^2 + \mu_y^2 + C_2}$, $c(x,y) = \frac{2\sigma_x \sigma_y + C_1}{\sigma_x^2 + \sigma_y^2 + C_2}$, $l(x,y) = \frac{\sigma_{xy} + C_3}{\sigma_x \sigma_y + C_3}$, $\mu_x, \mu_y, \sigma_x, \sigma_y, \sigma_{xy}$, are the local means, standard deviation and cross-covariance for images x, y. C_1, C_2 and C_3 are constants, and α, β, γ are default exponents [12], [13].

III. PROPOSED METHODOLOGY AND ALGORITHM

In this section, an informal way of describing the logical steps and main procedures of our algorithm is presented. The main scope is to predict the skin area surrounding the skin lesion, therefore proposing an algorithm in eight steps.

Prior to the prediction, the dermoscopic images with the local graph cut method were segmented (step 1). Image segmentation is a crucial step in image processing as it permits the analysis of only a portion of the image and eliminates redundant information. The mask that contains the area surrounding the skin lesion was projected using binarization images with the Otsu method (step 2), followed by the erosion and dilation morphological techniques, both of which used a square structuring element with a size of 100 (step 3). Because the aim was to analyze only the ROI, the background was removed (step 4). The template samples were obtained when images were split into subimages with a 100x100 size (step 5). Only the texture of the templates was checked to see if it was adequate for the area surrounding the skin lesion, so the templates were cropped from inside the ROI (step 6). In step 7, the NCC procedure was applied for the detection of the correlation of the pattern between template and ROI; the maximum of the magnitude spectrum was detected; the coordinates were kept; and the area was marked with yellow squares. The last step is supposed to compute the SSIM between each template and the detected area surrounding the skin lesion, marking with a red square the area on the original image if the SSIM index exceeds a set threshold. For an easy understanding of algorithm pseudocode, the name of the variable and keywords is specified in italic characters, the input, output and the steps in bold characters, and for each step are pointed out the name of obtaining images, figures and used equation.

IV. ALGORITHM PSEUDOCODE

Input: Original image from 7-Point dataset (I, Fig. 1(a))
Output: Prediction of melanoma progression (Fig. 5)
Step 1: Local Graph Cut Segmentation (Fig. 1(b))
Step 2: Binary images (*Im*, Fig. 2(a))
Step 3: Mask detection
    3.1 Eroding image *Im* with square morphological structuring element having side of 100 (*Im1*)
    3.2 Dilating image *Im* with square morphological structuring element having side of 100 (*Im2*)
    3.3 *Im3= Im1 xor Im2* (Fig. 2(b))
    3.4 Overlapping of images *I* and *Im3* (Im4, Fig. 3(a))
Step 4: Removing of the background and obtaining the region of interest (*Im5*, Fig. 3(b))
Step 5: Split image *Im5* into squares 100x100 size (*Im6*, Fig. 4(a))
Step 6: Detect the squares (*qi*) inside region of interest, in *Im6* are marked with red color
Step 7: *for each qi*
    if qi∈ROI then
        ai=NCC_procedure(qi, Im4) and mark with yellow color squares in Fig. I the the area to which the magnitude spectrum is maximum (Figs. 4(a), 4(b), and equation (1))
    end if
  end for
Step 8: *for each qi*
    if procedure_SSIM(qi, ai) >0.75 then
        Mark with red color squares in Fig. 1 the prediction (Fig. 5, and equation (2))
    end if
  end for

The methods implied in the results of the algorithm for each step are described in the following paragraphs, and processed images are shown in Figs. 1–5.

The first step in the algorithm is dedicated to image segmentation with the GCS method, which is semiautomatic segmentation that can be used to segment an image into foreground and background pixels. In this case, the users interact with the original image (Figure 1(a)) and draw a rectangle around the skin lesion. The GSC acts only inside the rectangle and segments the ROI. The results of the GCS method are shown in figure 1(b).
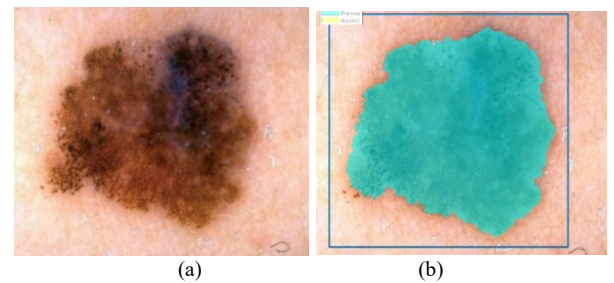

(a)   (b)

Fig. 1. Examples of some detected regions of the melanoma area after processing operation; (a) Original image; (b) Local graph cut segmentation method;

The second step proposed a transforming of the segmented image into a binary image. The Otsu method [14] is more adequate thresholding method because it finds an optimum

threshold from a grayscale image. This method supposes using the grayscale histogram, computing the cumulative distribution function, computing the mean intensity value of the grayscale image, also measuring the variance between the foreground and background regions, and finding the threshold value that maximizes the variance between the foreground and background regions. The binary image is shown in Fig 2(a).

In step 3, detecting the shape of a mask with dilation and erosion morphological operations was performed. When the mathematic morphological transform is applied to binary images, in this case, Fig. 2(a), a structural element (ES) is required to be defined. We proposed for ES to be a square [15], ED probes the border of the object, and after dilation and erosion operations, the contours of the lesion are detected. In order to detect the peritumoral area between the dilated and eroded images, the XOR logic operator was applied. The size of the peritumoral area between the dilated and eroded images is shown in Fig. 2(b) The mask is in a binary image, so that is necessary as in a white image is to fill with the texture of the image; in this sense, the original image and mask were overlapped. This operation was performed because only the texture of the peritumoral area should be analyzed by the algorithm. Fig. 3(a) shows the area to be analyzed.

An accurate result of image segmentation leads to the best detection of the peritumoral area, which is approximately similar to the texture of the lesion if the background of the lesion is removed. An overlapping between the images from Fig. 2(a) and the original image transformed into grayscale has the result of an image without background. The result is pointed out in Fig. 3(b), and in the algorithm is step 4.
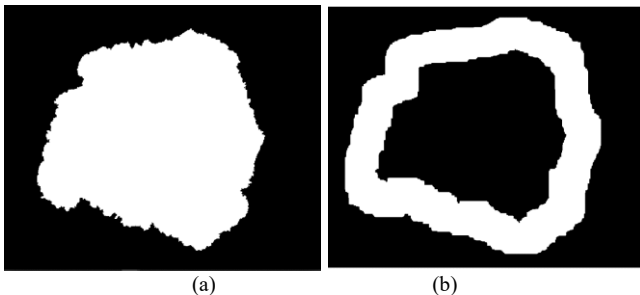

(a)   (b)

Fig. 2. (a) Binary images; (b) The peritumoral mask.
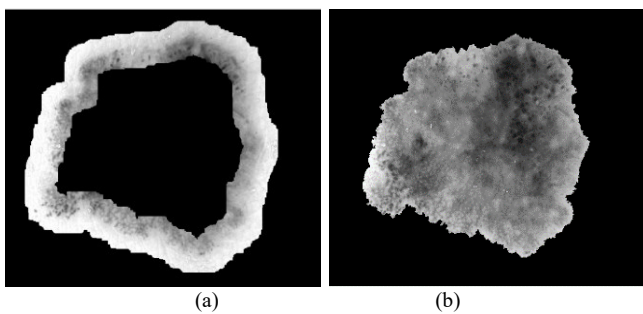

(a)   (b)

Fig. 3. (a) Peritumoral area of the melanoma; (b) Region of interest of melanoma.

The images have been resized so that they can be divided into 25 squares with the same lengths. In fig. 4(a), the squares analyzed are shown, and step 6 of the algorithm specifies the procedure. This step was necessary because the algorithm checked only the area that belonged to the lesion; the squares that contained the pixels from the background were removed. The concern was to detect the squares filled by pixels from the lesion. These squares are pointed out with a red border, and in

the next steps, only these squares were taken into account. The size of the squares was chosen so that they would be equal to the size of the peritumoral area.

For each square with a red color border determined in the previous step, e.g., in Fig. 4 (a), the NCC procedure was applied to detect the similarity between the pixels that belong to the squares from inside the lesion and the area that belongs to the texture of the peritumoral area. The number of ROIs detected in the peritumoral area is equal to the number of squares with a red border. In step 7, we check all detected ROIs, and with NCC, we find all the peaks in cross-correlation. In Fig. 4(b), these maximums are pointed out. As seen, the maximum magnitude spectrum is verified only in the peritumoral area. The peak is considered the centroid of the main square; its coordinates are kept, and the squares on the original images are marked; instead, not all determinate peaks reflect the best similarity, so eventually the SSIM index is proposed for computing the similarity between the texture of the main square and the square belonging to the lesion.

The computation of SSIM between the ROIs leads to keeping only the area for which the SSIM > 0.75; in Fig. 5, the overleap is indicated by the red square of the predicted area. More situations are recorded in our experiment when only one, two, or three predicted areas are highlighted, and all results are synthesized in the section results and discussions.
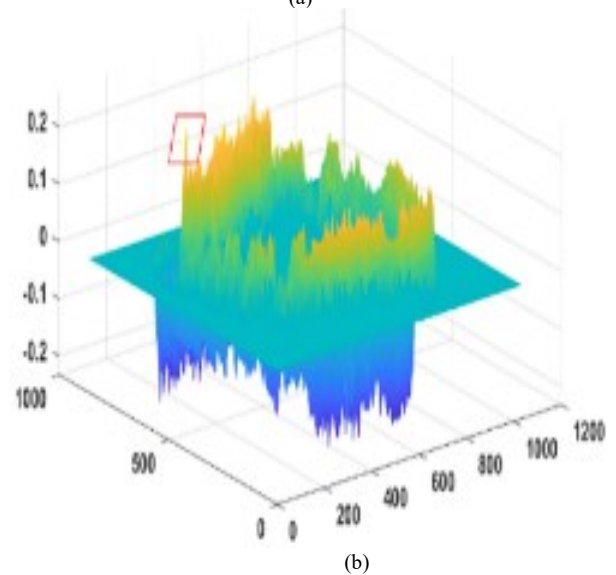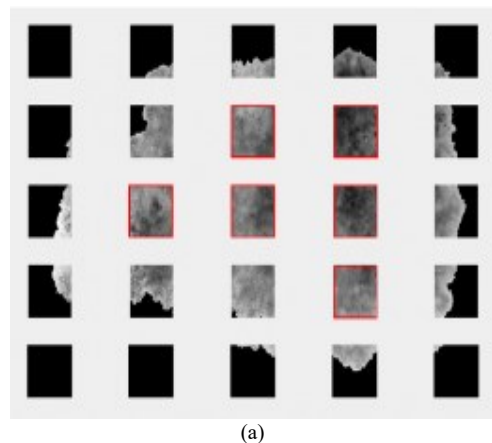

(a)

(b)

Fig. 4. (a) Split in squares with 100x100 size; (b) Typical examples of magnitude spectrum of dermoscopic images.
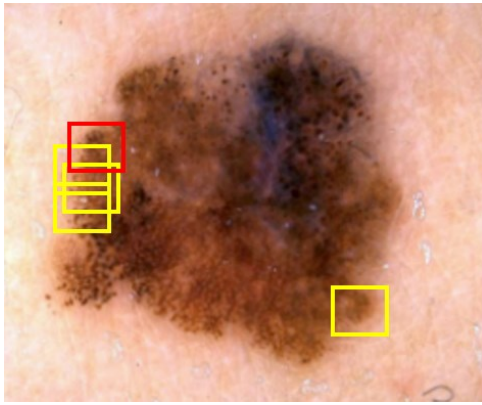
Fig. 5. The original images with predicted area.

V. Results and discussions

The measure of resource and performance of an algorithm is expressed as a function of the size of the input; in this case, two datasets were proposed. (297 melanoma, https://derm.cs.sfu.ca/), PH2 (40 melanoma, https://www.fc.up.pt/addi/ph2%20database.html).

The hardware and software resources influence the algorithm's performance, so it was tested on two personal computers with different architectures, (i) Intel(R) Core(TM) i7-8550U CPU @ 1.80GHz 1.99 GHz , 8BG RAM, (ii) Intel(R) Core(TM) i7-1065G7 CPU @ 1.30GHz 1.50 GHz, 16.0 GB RAM, the programming environment was Matlab R2018a with Image Processing Toolbox.

The algorithm contains three main procedures: local graph cut segmentation, NCC, and SSIM, as it is known that these are sequences of functions with the aim of solving a processing problem. The proposed algorithm contains a complex segmentation method, and all images were resized at 500x500. The time-consuming can be influenced by a number of procedures, image size, and hardware architecture. If the number of templates that belong inside the ROI increases, the time consumption decreases. Moreover, the algorithm was tested with a 100x100 template size. It was computed per image, and from each image there were chosen templates that were slid on the peritumoral area, the number of each template being different as it depended on the melanoma size. The average value per image in Table I is stored.

TABLE I. Detail About Time Consumption And Storage Spaces

Image database	Average time (s)/image	Type images	Storage Space database (MB)	Storage Space scripts (KB)
7-Point	(i) 4.09	jpg	6.35	1.67
	(ii) 3.98			
PH2	(i) 4.17	bmp	47.5	
	(ii) 3.87			

With the resources presented in the previous paragraphs, the algorithm provides the result from Table II. It stores the number of images in the function by SSIM value for each image database. Furthermore, it specifies the number of predicted areas. In the last step of the algorithm, the SSIM index is computed, and the trend in the spreading of melanoma

is detected if the template is similar to the area of the surrounding melanoma.

TABLE II: Number of Predicted Sample Images

Image database	SSIM>0.75/ number of samples predicted		
	1	*2*	*3*
7-Point	120	58	98
PH2	15	11	6

Conclusion

In this work, an algorithm for the processing of dermoscopic images was implemented. The novelty consists in creating the mask surrounding the melanoma and predicting the trend in the spreading of melanoma. The performance of the algorithm depends on the type of image and the size of the melanoma. The proposed algorithm can be integrated into computer-based diagnostic systems, which are very useful for clinicians and experts in order to get significant information about the prediction of the advance direction of the peritumoral areas. In future research, we propose to extend the study to different medical image types and diagnostics.

References

[1] K.V. Laikova, V.V. Oberemok, A.M. Krasnodubets, N.V. Gal'chinsky, R.Z. Useinov, I.A. Novikov, Z.Z. Temirova, M.V. Gorlov, N.A. Shved, V.V. Kumeiko et al., "Advances in the Understanding of Skin Cancer: Ultraviolet Radiation, Mutations, and Antisense Oligonucleotides as Anticancer Drugs," Molecules, 2019, vol. 24, pp. 1516.

[2] S. Mustafa, A. B. Dauda and M. Dauda, "Image processing and SVM classification for melanoma detection," in International Conference on Computing Networking and Informatics (ICCNI), 2017, Lagos, pp. 1–5.

[3] S. Moldovanu, C.D. Obreja, K.C. Biswas and L. Moraru, "Towards Accurate Diagnosis of Skin Lesions Using Feedforward Back Propagation Neural Networks Diagnostics," 2021, vol. 11, pp. 936.

[4] H. Xu, L. Liu, X. Lei, M. Mandal and C. Lu, "An unsupervised method for histological image segmentation based on tissue cluster level graph cut," Comput. Med. Imaging Graph., 2021, 93, pp.101974.

[5] E. Aptoula and S. Lefèvre, "A comparative study on multivariate mathematical morphology," Pattern Recognit., 2007, vol. 40(11), pp. 2914-2929.

[6] B. Quan, X. Liu, S. Zhao, X. Chen, X. Zhang and Z. Chen, "Detecting Early Ocular Choroidal Melanoma Using Ultrasound Localization Microscopy," Bioeng., 2023, vol.10, pp. 428.

[7] S. Liu, B. Yang, Y. Wang, J. Tian, L. Yin and W. Zheng, "2D/3D multimode medical image registration based on normalized cross-correlation," Appl. Sci., 2022, vol.12, pp. 2828.

[8] S. Chatterjee, D. Dey, S. Munshi and S. Gorai, "Extraction of features from cross correlation in space and frequency domains for classification of skin lesions," Biomed. Signal Process Control, 2019, vol. 53, pp. 101581.

[9] X. Song , S Guo., L.Han, L. Wang , W. Yang , G.Wang and C.A. Baris ,,Research on hair removal algorithm of dermatoscopic images based on maximum variance fuzzy clustering and optimization criminisi algorithm," Biomed. Signal Process. Control, 78 (2022), pp. 103967.

[10] A. Willenberg, A. Saalbach, J. Simon and U. Anderegg, "Melanoma cells control HA synthesis in peritumoral fibroblasts via PDGF-AA and PDGF-CC: Impact on melanoma cell proliferation," J. Invest. Dermatol., 2012, vol.132, pp. 385–393.

[11] J.P. Lewis, "Fast Normalized Cross-Correlation," Vis. Interface, 10, 1995, pp. 120-123.

[12] W. Zhou, A. C. Bovik, H. R. Sheikh and E. P. Simoncelli, "Image Qualifty Assessment: From Error Visibility to Structural Similarity," IEEE Trans. Image Process, Vol. 13(4), 2004, pp. 600–612.

[13] M. Punga, S. Moldovanu and L. Moraru, "Structural similarity analysis for brain MR image quality assessment" in AIP Conference Proceedings, 2012, vol. 1634, pp. 137.

[14] J. Ramya, H.C. Vijaylakshmi and H.M. Saifuddin, „Segmentation of skin lesion images using discrete wavelet transform," Biomed. Signal Process. Control, 69 (2021), pp. 102839.

[15] S. Moldovanu, F. A. Damian and L. Moraru, "A new algorithm for melanomas contour detection based on morphological operators," Annals Of The University Of Craiova Series: Automation, Computers, Electronics and Mechatronics, Vol. 14 (41), , 2018, pp. 41-44.